

ARTICLE TEMPLATE

## The Effect of Path Curvature on the Stability of Reversing Truck–Semitrailer in the Presence of Feedback Delay

Levente Mihályi<sup>a</sup> and Dénes Takács<sup>a,b</sup>

<sup>a</sup>Department of Applied Mechanics, Faculty of Mechanical Engineering, Budapest University of Technology and Economics, Műegyetem rkp. 3., Budapest H-1111, Hungary;

<sup>b</sup>HUN-REN–BME Dynamics of Machines Research Group, Műegyetem rkp. 3., Budapest H-1111, Hungary

### ARTICLE HISTORY

Compiled September 17, 2024

### ABSTRACT

Stability analysis of the low-speed reverse motion along clothoid curve is presented for the truck–semitrailer combination. The single-track kinematic model supplemented with the steering system and the lower-level controller is applied. A higher-level controller is designed to stabilize the reverse motion of the vehicle. Linear state feedback with time delay is used with feedforward term to force the vehicle to the desired path. The linear stability analysis is done by semi-discretization and D-subdivision methods to determine the optimal control gain setup. The effects of path curvature and time delay on the stability are investigated and verified via numerical simulations. Results are validated via experiments using a small-scale test rig.

### KEYWORDS

truck–semitrailer; reversing; stability analysis; time delay; clothoid; experimental validation

## 1. Introduction

Autonomous vehicles represent not only the progress of modern engineering but also optimization in terms of safety, traveling speed, and operating costs. While ensuring safety is a duty, shortening travel time and reducing costs may be the next level in the competition among designers and developers in the automotive industry. The main idea behind developing self-driving functions for articulated vehicles may be the same as for passenger cars, however, it usually implies different and more complex tasks for engineers. One of the main difficulties in developing safety functions for trailers is the lack of precise sensors (due to additional costs) and the communication between the truck and the trailer. To solve this problem, an estimation method of the articulation angle, based on truck data only, is presented in [1]. In the case of long transport distances, where most of the trip runs on highways, an important task to be solved is to operate long convoys with only one human driver in the front. Utilizing the advantages of vehicle platooning, such as reducing fuel consumption and improving

---

Levente Mihályi, mihalyi@mm.bme.hu, ORCID: 0009-0007-5901-0624

Dénes Takács, takacs@mm.bme.hu, ORCID: 0000-0003-1226-8613

traffic efficiency is crucial, see [2,3].

Another area of interest is realizing complicated maneuvers with truck–trailer systems. Engineers have to pay special attention to reversing articulated vehicles. Unless it can easily lead to catastrophic accidents (e.g., the Jackknifing phenomenon [4,5]) because this motion is unstable in any condition without active control. It may seem an obvious option to install independent steering mechanism on the axle of the trailer – also called as actuated trailers – in order to actively control the articulated part of the vehicle system. This application can be helpful in realizing low-speed narrow turns [6], or even high-speed maneuvering, see [7]. However, due to the lower initial and operating costs, passive trailers, when only the towing truck has actuation, are probably more convenient to develop, even with their more complicated controllability [8]. In this study, only passive trailers are considered. Current rudimentary control assist features for heavy-trucks only help human drivers, not entirely solve those time-consuming maneuvers [9], so there is a long development process until fully automated trucks are reached.

Collision avoidance is one task to solve in order to accomplish complicated maneuvers in a warehouse environment [10]. Auto-parking systems are also developed, see [11]. Parallel and perpendicular reverse parking is unavoidable at docking stations [12–14]. Transport companies suffer from the dwelling time problem, which would be improved if autonomous trucks were installed at the loading bay. This development could also save money for the companies and would allow the drivers to spend their driving time actually traveling. This feature can park the vehicle in a narrower parking location, nearer to each other. Furthermore, with the possibility of connected vehicles (communication between the vehicles nearby), it can operate well-synchronized without any human actuation.

The subject of our research is a truck–semitrailer combination, which is the most common vehicle type of freight transportation worldwide. Our paper deals with the simplified model of a truck–semitrailer, and the purpose of the paper is to design and analyze a control scheme for stabilizing the reverse motion and keeping the vehicle system on a prescribed path. The method is extended to solve the path-following problem along clothoid curve [15], which supports the smooth operation of articulated vehicles in self-driving mode. The time delay of the control loop consisting of data processing is also considered a significant contribution. Examining its effect on stability shows that neglecting the processing time often seems irresponsible. A single-track kinematic model is used [16,17].

The mechanical model is introduced in Section 2. Section 3 discusses an improved and helpful vehicle control situation, enabling the examination of general path-following control. The main results of the path-following problem are linear stability charts. Based on these graphs, three control gain tuning methods are compared using nonlinear simulations in Section 4. Furthermore, spectral analysis is also investigated to estimate the frequency at which the loss of stability happens. Finally, the presented results are validated via a small-scale test rig in Section 5.

## 2. Mechanical model

In order to analyze the path-following problem of the truck–semitrailer combination, equations of motion in the path-reference frame are needed. Let us first introduce the single-track mechanical model of the vehicle system shown in Figure 1. The chassis of the truck and the trailer are replaced by two rigid rods – neglecting the lateral

extension of the vehicle – and the wheels are considered as massless rigid wheels with single contact points with the ground (see [18]). It is worth mentioning that more complicated models, also including tire dynamics, would be justified if the investigation were extended to high-speed maneuvering, or aggressive accelerating and turning. The assumption of rigid wheels may be appropriate in this study since we focus on low-speed maneuvering along a path with relatively small curvatures, which would generate small slide slip angles at the wheels on a real vehicle, too. Of course, in the case of multi-axle trailers and/or multi-axle trucks, relevant slide slip at the wheels can occur even in the situations we investigate in this study, and an accurate tire deformation description is unavoidable. Hence, we exclude the multi-axle trailers/trucks from our examination.

The truck and the trailer are connected at kingpin K. Points F, R, and T represent the rigid wheels at the front and rear axles of the truck and the axle of the trailer, respectively. The geometrical parameters are the wheelbase  $l$ , the distance  $a$  of the kingpin and the rear axle of the truck, and the distance  $L$  between the kingpin and the axle of the trailer, see Figure 1. The mechanical model represents a general truck–trailer combination, however, it is important to point out that in the case of a real truck–semitrailer, the distance between the rear axle and the kingpin is negative (i.e.,  $a < 0$ ). The steering angle  $\delta$  of the front axle F refers to the only actuated variable of the system. The position and the orientation of the vehicle system are expressed by the coordinates  $x_R$  and  $y_R$  of the rear axle center point R, by the yaw angle  $\psi$  of the truck, and by the angle  $\varphi$  of the trailer measured from the longitudinal axis of the truck.

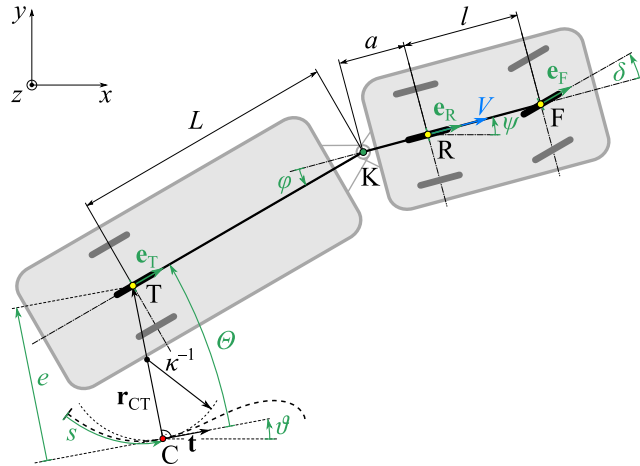


**Figure 1.** Single-track kinematic model of a truck–semitrailer with the illustration of the path-following problem.

The equations of motion are rooted in the kinematic constraints of the rolling rigid wheels. These constraints ensure that the velocity vectors  $\mathbf{v}_F$ ,  $\mathbf{v}_R$  and  $\mathbf{v}_T$  of points F, R, and T are parallel to the proper wheel plane, respectively, which are described by unit vectors  $\mathbf{e}_F$ ,  $\mathbf{e}_R$  and  $\mathbf{e}_T$  shown in Figure 1. That is, the kinematic constraints are formulated in

$$\mathbf{v}_F \parallel \mathbf{e}_F : \quad \mathbf{v}_F \times \mathbf{e}_F = \mathbf{0}, \quad (1)$$

$$\mathbf{v}_R \parallel \mathbf{e}_R : \quad \mathbf{v}_R \times \mathbf{e}_R = \mathbf{0}, \quad (2)$$

$$\mathbf{v}_T \parallel \mathbf{e}_T : \quad \mathbf{v}_T \times \mathbf{e}_T = \mathbf{0}. \quad (3)$$

Another kinematic constraint is also considered in our study, namely, the longitudinal speed of the rear-wheel-drive truck is kept at the constant value  $V$ :

$$\mathbf{v}_R \cdot \mathbf{e}_R = V. \quad (4)$$

Note that the model can handle the negative sign of the longitudinal velocity  $V$ ; therefore, the sign of it defines whether the vehicle system moves forward ( $V > 0$ ) or backward ( $V < 0$ ). In this study, the reverse motion is examined, i.e., the sign of velocity  $V$  is always negative.

Finally, the kinematic constraints can be evaluated by substituting the expressed velocity vectors and unit vectors into (1)–(4):

$$\dot{x}_R \sin(\psi + \delta) - \dot{y}_R \cos(\psi + \delta) - \dot{\psi}l \cos \delta = 0, \quad (5)$$

$$\dot{x}_R \sin \psi - \dot{y}_R \cos \psi = 0, \quad (6)$$

$$\dot{x}_R \sin(\psi + \varphi) - \dot{y}_R \cos(\psi + \varphi) + \dot{\psi}a \cos \varphi + (\dot{\psi} + \dot{\varphi})L = 0, \quad (7)$$

$$\dot{x}_R \cos \psi + \dot{y}_R \sin \psi = V. \quad (8)$$

These form a system of linear equations with respect to the so-called generalized velocities  $\dot{x}_R$ ,  $\dot{y}_R$ ,  $\dot{\psi}$  and  $\dot{\varphi}$ .

By solving (5)–(8) for the generalized velocities, we obtain:

$$\begin{aligned} \dot{x}_R &= V \cos \psi, & \dot{y}_R &= V \sin \psi, & \dot{\psi} &= \frac{V}{l} \tan \delta, \\ \dot{\varphi} &= -\frac{V}{lL} (l \sin \varphi + (L + a \cos \varphi_2) \tan \delta). \end{aligned} \quad (9)$$

In the mechanical model, we also consider the dynamics of the steering system together with the lower-level controller. Namely, the steering mechanism is characterized by a one degree-of-freedom system, where the steering torque  $M_s$  is produced by a PD controller:

$$J \ddot{\delta} = M_s, \quad \text{where} \quad M_s = -P(\delta - \delta_{\text{des}}) - D\dot{\omega}, \quad (10)$$

where  $J$  is the effective mass moment of inertia of the steering system;  $P$  and  $D$  are the control gains. The desired steering angle  $\delta_{\text{des}}$  is determined by the higher-level controller that will be introduced in Section 3.2. Let us denote the steering rate by  $\omega$ . After rearranging the equation, one can read

$$\dot{\delta} = \omega, \quad \dot{\omega} = -p(\delta - \delta_{\text{des}}) - d\omega. \quad (11)$$

Hence, the notations  $p = P/J$  and  $d = D/J$  are the proportional and the derivative gains of the lower-level controller. Note that (11) is rescaled by the mass moment of inertia  $J$  so that the gains  $p$  and  $d$  may be considered as parameters independent of the size of the vehicle. The values of the gains used in our investigation are given in Table 1.

### 3. Path-following problem

The general path-following is inevitable in order to make maneuvers on the road or avoid obstacles. In this paper, we focus on the reversing motion of the truck–semitrailer combination, and we prescribe the path of the axle center point T of the trailer. The so-formed path-following problem is suitable for designing a controller that enables the steering of the vehicle to the docking station.

#### 3.1. Coordinate transformation

To obtain the equations of motion for realizing path-following control, the position of the axle T in the  $(x, y)$  ground-fixed coordinate system has to be expressed as a function of the generalized coordinates  $x_R, y_R, \psi$  and  $\varphi$ :

$$\begin{aligned} x_T &= x_R - a \cos \psi - L \cos(\psi + \varphi), \\ y_T &= y_R - a \sin \psi - L \sin(\psi + \varphi). \end{aligned} \quad (12)$$

Furthermore, a coordinate transformation is needed between the ground-fixed and the path-reference frames, as detailed in [18]. The new notations related to point C, the closest point on the prescribed path, are defined in Figure 1. The state vector develops as

$$\mathbf{x} = [s \ e \ \theta \ \varphi \ \delta \ \omega]^T, \quad (13)$$

where  $s$  is the path coordinate,  $e$  is the lateral deviation (i.e., the distance between points T and C), and  $\theta = \psi + \varphi - \vartheta$  is the yaw angle of the trailer relative to the path, also called as the angle error. Namely,  $\vartheta$  represents the angle of the tangent of the path at point C, which changes in time according to the traveling speed  $\dot{s}$  along the path and the path curvature  $\kappa$ , i.e.,  $\dot{\vartheta} = \kappa \dot{s}$ .

Based on [18], the transformation between the ground-fixed and the path-reference frames can be done by

$$\begin{aligned} \dot{s} &= \frac{\dot{x}_T \cos \vartheta + \dot{y}_T \sin \vartheta}{1 - \kappa e}, \\ \dot{e} &= -\dot{x}_T \sin \vartheta + \dot{y}_T \cos \vartheta, \\ \dot{\theta} &= \dot{\psi} + \dot{\varphi} - \kappa \dot{s}, \end{aligned} \quad (14)$$

where  $\dot{\psi}$  depends on the steering angle  $\delta(t)$  based on (9). The equations related to the relative yaw angle  $\varphi$  in (9) and to the steering mechanism in (11) remain the same in the transformed coordinate system. Finally, after substituting the velocities  $\dot{x}_T$  and  $\dot{y}_T$  of point T, i.e. the time derivatives of (12), into (14), the transformed governing

equations read

$$\begin{aligned} \dot{s} &= \frac{V}{1 - \kappa e} \left( \cos(\theta - \varphi) + \frac{a}{l} \tan \delta \sin(\theta - \varphi) \right) \\ &\quad - \frac{V}{1 - \kappa e} \left( \sin \varphi + \frac{a}{l} \cos \varphi \tan \delta \right) \sin \theta, \end{aligned} \quad (15)$$

$$\begin{aligned} \dot{e} &= V \left( \sin(\theta - \varphi) - \frac{a}{l} \tan \delta \cos(\theta - \varphi) \right) \\ &\quad + V \left( \sin \varphi + \frac{a}{l} \cos \varphi \tan \delta \right) \cos \theta, \end{aligned} \quad (16)$$

$$\dot{\theta} = \frac{V}{l} \tan \delta + \dot{\varphi} - \kappa \dot{s}, \quad (17)$$

$$\dot{\varphi} = -\frac{V}{lL} (l \sin \varphi + (L + a \cos \varphi) \tan \delta), \quad (18)$$

$$\dot{\delta} = \omega, \quad (19)$$

$$\dot{\omega} = -p\delta - d\omega + p\delta_{\text{des}}, \quad (20)$$

where one should substitute (15) and (18) into (17) to obtain the conventional form of the system of first-order differential equations. Here, we omit this step in order to shorten the formulas. Note that the curvature  $\kappa(s)$  may depend on the arclength, hence, (15)–(20) are all coupled together. However, using the state vector (13), (15)–(20) can be given in the control affine form

$$\dot{\mathbf{x}} = \mathbf{f}(\mathbf{x}) + \mathbf{g}(\mathbf{x})\mathbf{u}, \quad (21)$$

where the input  $\mathbf{u}$  refers to the desired steering angle  $\delta_{\text{des}}$ .

General path-following problem can be described and analyzed using these equations in the case of a truck–semitrailer. Curvature  $\kappa$  can depend on time (or on arclength, more precisely) arbitrarily. However, using a specific curve makes this change regulated.

### 3.2. Controller design

Varying curvature makes the linearized governing equations time-dependent, and stability analysis is complicated or impossible. So, in this paper, we design our controller for constant path curvature, and later, we apply this controller to real situations with the assumption that the curvature changes slowly.

In our study, the control of the reverse path-following of the truck–semitrailer combination is achieved by a hierarchical controller. The lower-level controller was already introduced in (11) as the model of the power steering system. The higher-level controller provides the desired steering angle  $\delta_{\text{des}}$  (as the only input to the system) by the control law:

$$\delta_{\text{des}}(t) = \delta_{\text{ff}} + \delta_{\text{fb}}(t). \quad (22)$$

The time-dependent feedback term  $\delta_{\text{fb}}$  is responsible for stabilizing the reverse motion along the path, while the curvature-dependent feedforward term  $\delta_{\text{ff}}(\kappa)$  improves the performance of the path-following. Note that in case of varying path curvature, the feedforward term  $\delta_{\text{ff}}(t)$  is time-dependent, and it could be calculated from the gov-

erning equations (15)–(20) evaluated along the desired path. In the general case, no analytical solution can be found for the feedforward term since the governing equations are nonlinear. Another option is the numerical solution of the so-formed equations system for specific paths, but the stability analysis of the time-dependent control system remains an unsolved problem. As stated previously, we limit our controller design to the constant path curvature case.

The linear feedback control  $\delta_{fb}$  consists of three proportional terms:

$$\begin{aligned} \delta_{fb}(t) = & -P_e e(t - \tau) - P_\theta \theta(t - \tau) \\ & - P_\varphi (\varphi(t - \tau) - \varphi^*), \end{aligned} \quad (23)$$

where  $\tau$  refers to the overall time delay of the control loop. It is primarily rooted in the sensory system, in the communication network and in data processing. Since the vehicle states are typically determined by image processing, and sensor fusion with signal filtering is applied, a significant time delay may arise in the control loop. Even in the case of automated vehicles, the time delay may be some tenth of second, or, in extreme cases it may reach one second (see, for example, [19]).

In the control law (23), the desired angle  $\varphi^*$  between the truck and the semitrailer is related to the steady state cornering motion that could be calculated by solving the governing equations with the conditions of zero derivatives of state variables. However, in the case of constant curvature, the steady state solution for the relative yaw angle  $\varphi^*$  and the feedforward steering angle  $\delta_{ff}$  can be determined by geometry as well, as shown in Figure 2. According to trigonometric formulas, they read

$$\varphi^* = \arctan \frac{1}{\kappa L} + \arccos \frac{a}{\sqrt{L^2 + 1/\kappa^2}} - \pi, \quad (24)$$

$$\delta_{ff} = \arctan \frac{l}{\sqrt{L^2 + 1/\kappa^2} - a^2}. \quad (25)$$

If curvature  $\kappa$  is infinitely large ( $\kappa \rightarrow \infty$ ), (25) leads to

$$\delta_{req} = \arctan \frac{l}{\sqrt{L^2 - a^2}}, \quad (26)$$

which gives the steering angle  $\delta_{req}$  that is required to realize steady state reversing on a path of arbitrary large curvature. Note that the extreme case  $\kappa \rightarrow \infty$  refers to the turning around the trailer's axle point T ( $\mathbf{v}_T = \mathbf{0}$ ).

If the steering angle limit  $\delta_{lim}$  of the truck for a specific vehicle combination is smaller than the required one ( $\delta_{lim} < \delta_{req}$ ), the maximum feasible path curvature is

$$\kappa_{max} = \frac{\tan \delta_{lim}}{\sqrt{l^2 - (L^2 - a^2) \tan^2 \delta_{lim}}}. \quad (27)$$

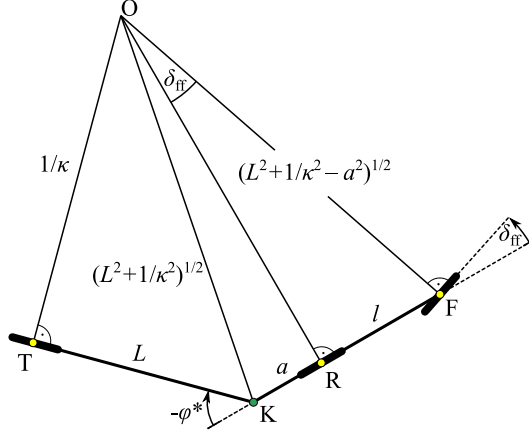


Figure 2. Geometry consideration of the steady state cornering.

### 3.3. Linear stability

In the case of constant curvature  $\kappa \equiv \text{const.}$ , (15) related to the arclength coordinate is decoupled from the rest of the governing equations. Hence, the state is reduced to:

$$\mathbf{x} = [e \quad \theta \quad \varphi \quad \delta \quad \omega]^T. \quad (28)$$

The linear state space representation of the mechanical system is obtained by the perturbation  $\tilde{\mathbf{x}}$  of the state variables, and perturbation  $\tilde{\mathbf{u}}$  of the input, so that

$$\mathbf{x}(t) = \mathbf{x}^* + \tilde{\mathbf{x}}(t), \quad \mathbf{u}(t) = \mathbf{u}^* + \tilde{\mathbf{u}}(t), \quad (29)$$

where  $\mathbf{x}^*$  and  $\mathbf{u}^*$  relate to the steady state motion, around which the linearization is done:

$$\begin{aligned} \mathbf{x}^* &:= [e^* \quad \theta^* \quad \varphi^* \quad \delta^* \quad \omega^*]^T \\ &= [0 \quad 0 \quad \varphi^* \quad \delta_{ff} \quad 0]^T, \end{aligned} \quad (30)$$

$$\mathbf{u}^* := [\delta_{ff}]. \quad (31)$$

Finally, the state space representation is obtained as

$$\dot{\tilde{\mathbf{x}}}(t) = \mathbf{A} \tilde{\mathbf{x}}(t) + \mathbf{B} \tilde{\mathbf{u}}(t - \tau), \quad (32)$$

where the system matrix  $\mathbf{A}$  and the input matrix  $\mathbf{B}$  (in this case, a vector) can be determined by

$$\mathbf{A} = \left. \frac{\partial \mathbf{f}}{\partial \mathbf{x}} \right|_{\mathbf{x}^*} \quad \text{and} \quad \mathbf{B} = \mathbf{g}(\mathbf{x}^*), \quad (33)$$

which are detailed in the Appendix.

The flatness of a truck–semitrailer combination as a mechanical model is proved, i.e., the controllability – via the steering rate of the truck and the driving velocity as inputs – is verified in [20,21]. It is worth mentioning, that there are different approaches

in the literature, e.g., where the steering rate is used as input in order to include some simplified model of the steering system, see also [22]. Here we use the desired steering angle as input, and the driving velocity is considered as constant. The condition of controllability – based on the system matrix  $\mathbf{A}$  and the control input vector  $\mathbf{B}$ , see (32), is checked numerically and fulfilled for the mechanical system presented in this paper.

The linear stability of the reverse motion ( $V < 0$ ) is analyzed based on (32). The steady state motion is considered to be stable if  $\mathbf{x}(t) \rightarrow \mathbf{0}$  after small perturbation as  $t \rightarrow \infty$ , i.e. the motion is asymptotically stable. The stability of the controlled reversing is investigated using the semi-discretization method [23]. This method allows us to investigate the effect of different parameters on linear stability. We especially focus on the effect of curvature and time delay on stability, so our calculations are made with fixed geometry parameters and longitudinal speed given in the second column of Table 1.

**Table 1.** Numerical values of the parameters for a real truck–semitrailer combination (second column) and for our small-scale experimental rig (third column).

Parameter	Real-scale	Small-scale
$V$	-1.5 m/s	-0.105 m/s
$a$	-0.8 m	0.05 m
$l$	3.5 m	0.24 m
$L$	10 m	0.22 m
$p$	300 1/s <sup>2</sup>	300 1/s <sup>2</sup>
$d$	34.6 1/s	34.6 1/s

We construct stability charts that give information about how to tune the feedback controller properly, as they are plotted in the plane of control gains  $P_\theta$  related to the angle error and  $P_\varphi$  related to the relative yaw angle, meanwhile, the control gain related to the lateral error is fixed at  $P_e = -5$  rad/m.

### 3.3.1. Relevance of steering dynamics

In the model of this study, the dynamics of the steering mechanism are included, see (10). The importance of this consideration is highlighted in Figure 3, where stability boundaries are plotted with black solid curves for considering and with black dashed curves for neglecting the steering dynamics. Linearly stable domains of control gains are shaded. A remarkable difference can be observed with respect to the area of stable control gain domain assuming moderate time delay in panel (a) or even significant time delay in panel (b). Moreover, in the case of  $\tau = 0.5$  s, the most stable gain configuration (marked by crosses) shifts as well, where the rightmost (critical) characteristic exponent has the smallest real part. Namely, vibrations may decay in time most rapidly at these control gain setups. The importance of including steering dynamics in the model is also shown in Section 5.2 by means of experimental results.

### 3.3.2. Effect of time delay

One of the parameters that has a significant effect on stability is the time delay, see Figure 4. Stability charts are displayed for three scenarios. Linearly stable domains are shaded. Gray area is referred to the zero time delay case, while different shades of blue represent delayed cases: a moderate time delay  $\tau = 0.1$  s and a significant time

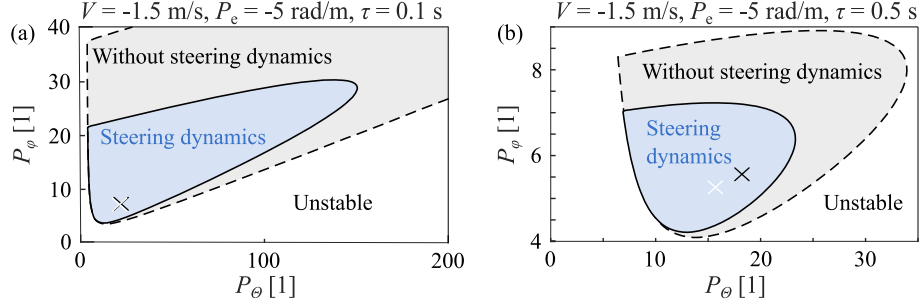


**Figure 3.** Stability charts for illustrating the effect of the steering dynamics in the case of moderate time delay (a) and significant time delay (b).

delay  $\tau = 0.5$  s. As the time delay is increased, the stable domain shrinks toward the origin. Crosses show the most stable gain configuration related to the different delays.

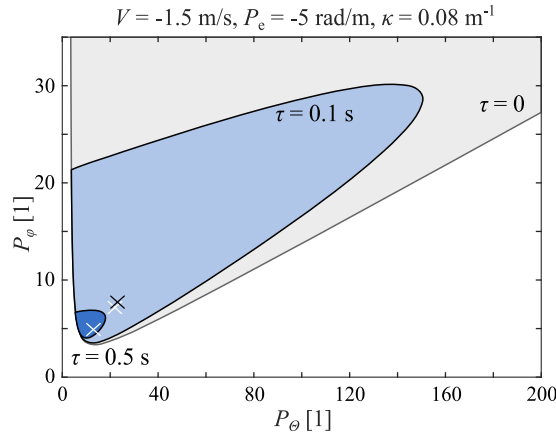


**Figure 4.** Effect of time delay on linear stability. Different shades refer to different time delay values. White crosses show the most stable gain configurations.

One option to reduce the harmful effect of time delay is slowing the vehicle down. However, commercial truck companies intend to increase the speed, especially during the loading procedure. Considering the time delay in the gain tuning method always results in better performance in reverse maneuvering. This is highlighted in Figure 5, where a comparison is presented between considering or neglecting the effect of time delay for both  $\tau = 0.1$  s in panel (a) and for  $\tau = 0.5$  s in panel (b). The real part of the rightmost (critical) eigenvalue is plotted, illustrating the performance of the real, not-delay-free system. Gray curves represent the case when the control gains are tuned for the most stable setup without considering the time delay, while blue curves denote the case when the time delay was precisely considered in the tuning method. As shown, the tuning based on the delayed mechanical model relevantly outperforms the delay-free model-based concept. The reverse motion can be realized at nearly twice longitudinal speed when the time delay is considered in the tuning.

### 3.3.3. Effect of curvature

In an analytical sense, stability can be assured for constant curvature only. However, if the change in curvature is relatively slow along the path, one can investigate stability by assuming quasi-stationary curvature. The stability charts in Figure 6 are generated

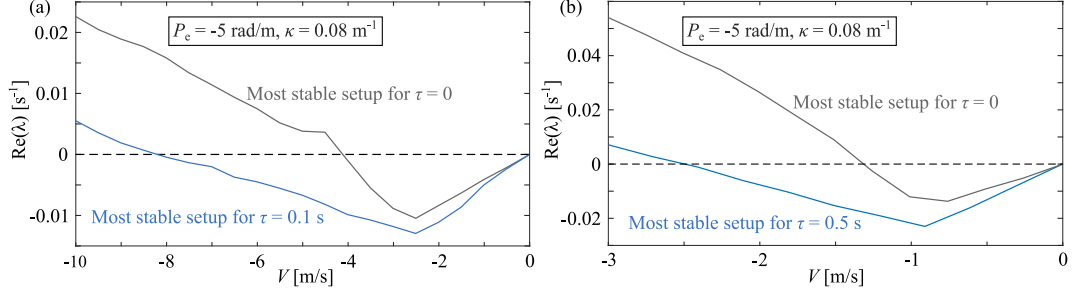


**Figure 5.** Comparison of the performance of reversing between two modeling methods: neglecting time delay (gray curves) and considering time delay (blue curves). Moderate  $\tau = 0.1$  s and significant  $\tau = 0.5$  s time delay values are considered in panels (a) and (b), respectively.

for two different time delays. Panel (a) refers to time delay  $\tau = 0.1$  s, while panel (b) is for  $\tau = 0.5$  s. Different shades of blue color refer to stable control gain setups for three different curvature values:  $\kappa = 0.08 \text{ m}^{-1}$ ,  $\kappa = 0.04 \text{ m}^{-1}$ , and  $\kappa = 0$  (i.e., straight line).

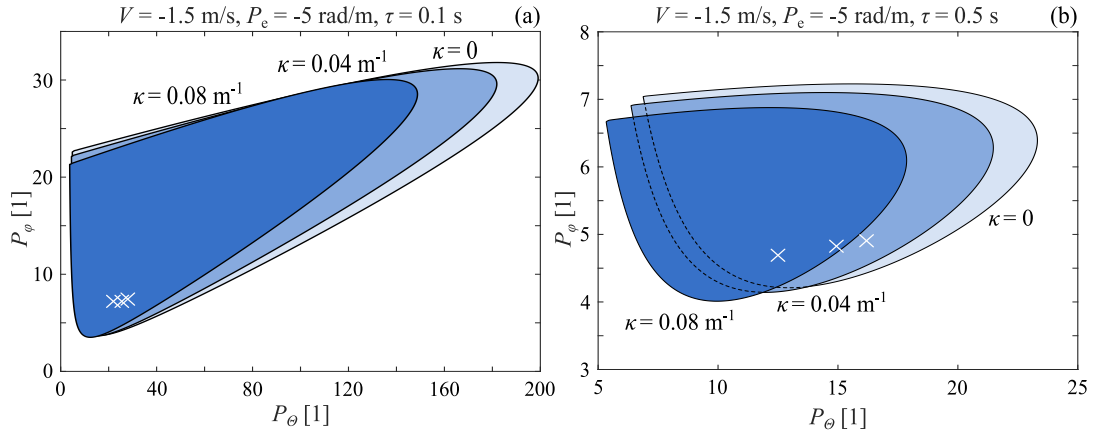


**Figure 6.** Stability charts for time delay  $\tau = 0.1$  s (a) and for  $\tau = 0.5$  s (b) for three different curvatures. The largest area is for zero curvature, i.e., straight line (lightest blue); and smaller stable domains (darker blue) belong to greater curvatures (sharper turns). White crosses denote the most stable gain setups for each curvature value.

As can be observed in Figure 6, the area of the stable domain shrinks as the curvature increases.

It is worth mentioning that in the case of constant curvature, there will always be a stable domain regardless of how large the curvature is. This statement is true when the required steering angle  $\delta_{\text{req}}$  in (26) is smaller than the steering angle limit  $\delta_{\text{lim}}$  of the truck. In the case of the geometry used in our study (Real-scale parameters in Table 1), the required steering angle is  $\delta_{\text{req}} = 19.3^\circ$ . Considering a typical steering angle limit  $\delta_{\text{lim}} = 35\text{--}40^\circ$  (see [24]), there is no limitation on the path curvature.

The location of the most stable gain setups (white crosses) has a crucial role in the performance of the controller. For the smaller delay (panel (a)), the most stable setups are involved by the stable domains of all the considered curvatures. This means that one can fix the control gains at any of the most stable setups, and the steady state motion remains stable independently from the path curvature within the investigated range. Of course, the performance of the controller will depend on the actual curvature. If better control performance is intended, adaptive gain configurations may be used.

For the large time delay (panel (b)), the use of adaptive control gain strategy is inevitable since the most stable control gain setup of a certain curvature may be located outside of the stable domain for a different curvature value. Another possibility is to find a less stable gain setup, which is located inside the stable domains for all curvatures. However, unwanted oscillations may appear since this fixed gain setup can be situated near the stability boundaries for certain curvature values. Thus, adaptive gain tuning based on stability charts seems to be beneficial, but mainly when the time delay  $\tau$  is relatively large.

#### 4. Simulations

In order to test our controller for realistic maneuvers, simulations are carried out where the path has varying curvature. Choosing the appropriate type of geometry curves to be followed by the vehicle is a crucial task. One common and well-tryed method in road and railway design is the clothoid curve. Its helpful property is that the curvature changes linearly along its arclength, which makes the connection between straight and curved segments smooth. Our path-designing is based on clothoids as well. Namely, we generate paths based on the method of [15], which can create a path with three segments for a given initial and final pose (i.e., position and orientation) with arbitrary curvature values at the starting and ending points.

The maneuver to be analyzed is a U-turn in reverse ( $V < 0$ ) with a truck–semitrailer. Although not the most common, it is a useful maneuver in docking stations and suitable for verifying the performance of our path-following controller. The maneuver used for the demonstration is shown in Figure 7(a), consisting of three clothoid arcs and a straight line connected to the end of it. The desired path is marked by the black dashed line, and a simulated trajectory (explained later) is plotted by the blue solid line. Figure 7(b) shows the change in curvature along the path.

A comparison between different control gain tuning strategies can be seen in Figure 8, where time histories of simulations are displayed. The simulations were executed by solving the nonlinear equations of motion (15)–(20) using the Matlab built-in solver `dde23` with adaptive time stepping. This method is based on the explicit Runge-Kutta method and is suitable for solving delay differential equations with constant delays. The initial conditions are set in accordance with the steady state related to the starting point, where the curvature is zero, i.e.,  $\mathbf{x}^* = \mathbf{0}$ .

In Figure 8(a)–(e), the time histories of the state variables, i.e., the lateral deviation  $e$ , the angle error  $\theta$ , the relative yaw angle  $\varphi$  between the truck and the trailer, the steering angle  $\delta$  and steering rate  $\omega$  are plotted for three alternative gain tuning approach with different colors. In panel (f), the curvature  $\kappa$  of the desired path is plotted versus the time  $t$ . The largest occurring curvature is  $\kappa = 0.08 \text{ m}^{-1}$ , and the assumed time delay in the control loop is  $\tau = 0.5 \text{ s}$ , so this relates to the stability chart in Figure 6(b).

In Figure 8, the yellow dashed line refers to the case when the control gains are set to the most stable point of zero curvature, i.e., for reversing along a straight line. As can be observed, this approach is not acceptable since the motion becomes unstable. This conclusion is consistent with the result of the theoretical stability analysis in Figure 6(b) because the optimum for zero curvature is in the unstable region of the largest occurring curvature.

Orange thin curves in Figure 8 relate to the most stable control gain setup of the largest occurring curvature value. The performance of the controller can be accepted

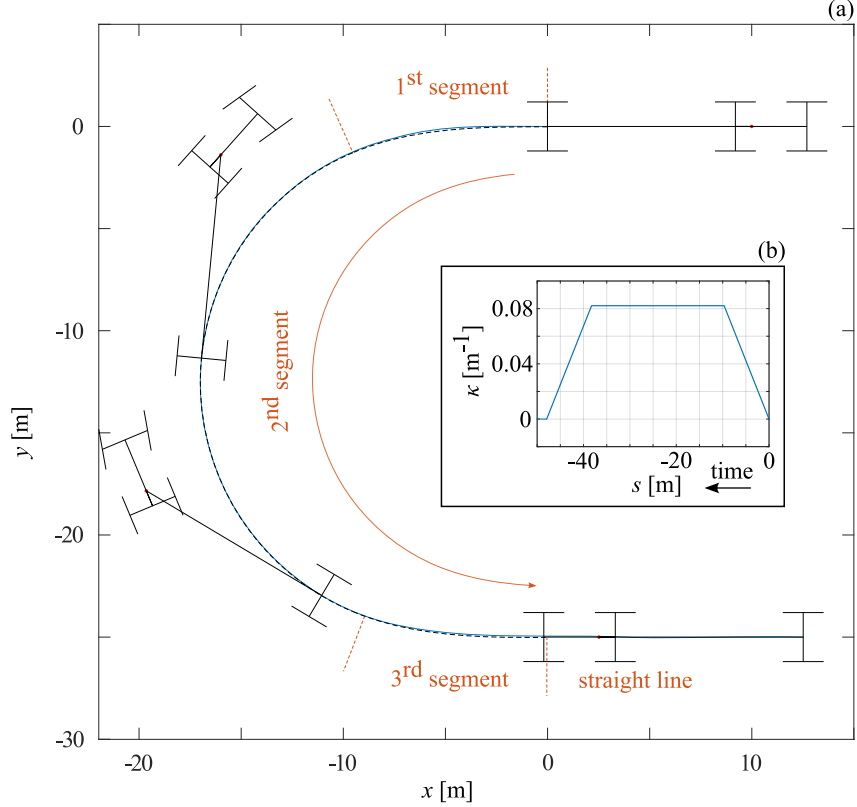


**Figure 7.** (a) The trajectory of a U-turn in reversing ( $V < 0$ ) – consisting of three clothoid arcs and a connected straight line segment – with the schematic figure of the vehicle combination in some specific time steps. The blue solid line is a simulated track of the midpoint of the trailer’s axle (point T). The black dashed line is the desired path, and the orange dashed markers are the separators between the path segments. (b) The curvature changes linearly along the path.

because the maximum value of lateral deviation  $e$  is under 0.1 m, which is admissible due to the large dimension of the vehicle combination. However, undesired oscillations appear near the connection between the clothoid and the straight line segments, around at 40 s.

Blue thick curves in Figure 8 show the adaptive control gain tuning, i.e., when we continuously vary the control gains by a lookup table and set them based on the most stable control gain setup of the actual curvature. This approach produces the best performance in our simulation. Although the maximum lateral deviation  $e$  is in the same range as in the second case, the unwanted oscillation does not appear at the end of the clothoid curve. In each of the graphs, the vertical dashed lines separate the curve segments according to the trajectory in Figure 7.

It is important to mention that in the final position of the reversing maneuver, the lateral deviation  $e$  and the angle error  $\theta$  are approximately zero so that the vehicle combination is possible to place properly to the docking station. Moreover, another crucial requirement is satisfied in the simulation, namely, the steering angle does not exceed the 35–40° limit [24]. The steering angle  $\delta$  is shown in Figure 8(d), where the maximum value of it is  $\delta = 0.588 \text{ rad} = 33.7^\circ$ .

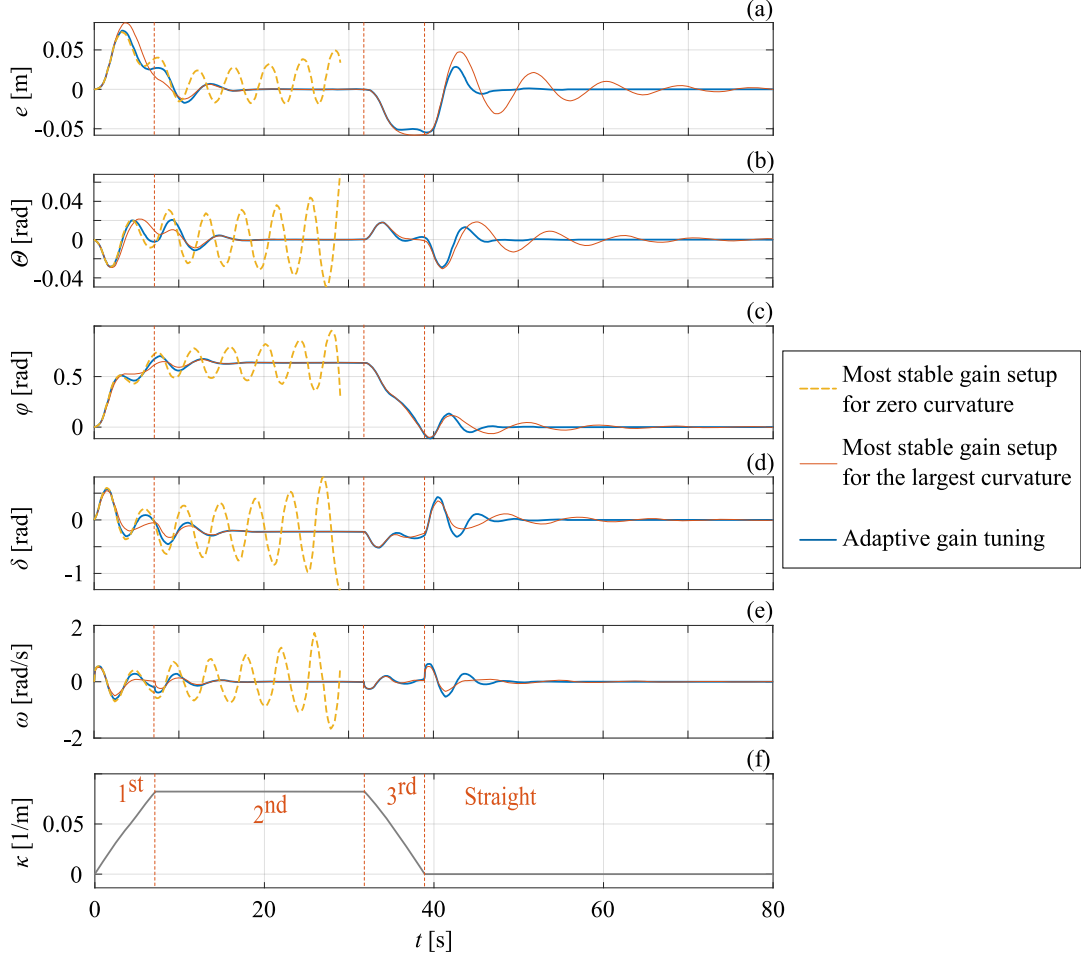


**Figure 8.** Simulation results with time delay  $\tau = 0.5$  s and lateral deviation gain  $P_e = -5$  rad/m to demonstrate three gain tuning methods: gains fixed to the most stable setup of the straight motion (yellow dashed line), gains fixed to the most stable setup of the largest curvature (orange thin line), and adaptive gain tuning based on the most stable setups of different curvatures (blue thick line). Vertical dashed lines separate the three segments of clothoid curve and the straight part.

## 5. Small-scale experiment

To validate the mechanical model and the theoretical results (especially the effect of time delay) a small-scale test rig is used, see Figure 9. Note that the geometric parameters of the small-scale vehicle are inconsistent with the parameters of the real truck-trailer system that was used in the former sections to highlight results for practically relevant vehicle parameters. For example, the distance  $a$  between the hitch point and the rear axle is positive in our experiment and negative for the real vehicle system, see Table 1. However, this does not violate the validity of our theoretical results; namely, the effect of time delay is similar for any parameter setup. This is shown in this section, where stability charts and theoretical vibration frequencies are validated for different time delays.

### 5.1. Test rig

According to the narrow conveyor belt, only maneuvers that require limited space can be performed. So, only the rectilinear motion is investigated via experiments. In the experiments, the towing vehicle is attached to the conveyor belt by a special suspension that fixes only the longitudinal position of the vehicle, thus ensuring the constant reversing speed as the belt goes forward, and at the same time, it maintains all the other degrees of freedom (lateral and vertical movement and rotations around the three axes) to be free.

The vehicle system is actuated only by the steering angle of the towing vehicle, which input is calculated using three sensors: a linear encoder and two angle sensors (one for the yaw angle of the truck and the other for the relative yaw angle between the truck and the trailer). Since rectilinear motion is a special case of the path-following motion along clothoid arcs, the same algorithm for producing the desired steering angle can be used, see (22)–(23). In the case of tracking a straight line, the curvature  $\kappa$  is considered zero, i.e., the feedforward term is zero.

The sensor data is processed by NI CompactRIO Systems with a sampling frequency of 1 kHz. However, due to the applied filters in the sensory system, the minimum time delay is about  $\tau = 0.1$  s, which can be further increased by adding extra time delay with 1 ms resolution in higher-level control. The desired steering angle is calculated based on these delayed signals. Then it is sent to the steering system, where the lower-level controller of our mechanical model is represented by the in-built controller of the steering servo motor. The gains  $p$  and  $d$  of this controller were identified by the measured responses of the steering system to different unit-step input signals. These values were also used in preliminary sections for the real-scale vehicle since the gains  $p$  and  $d$  are already scaled by the mass moment of inertia of the steering system, see Table 1. It is worth noting that in accordance with our mechanical model, the time delay in the lower-level controller can be neglected thanks to the high sampling frequency of the steering servo.

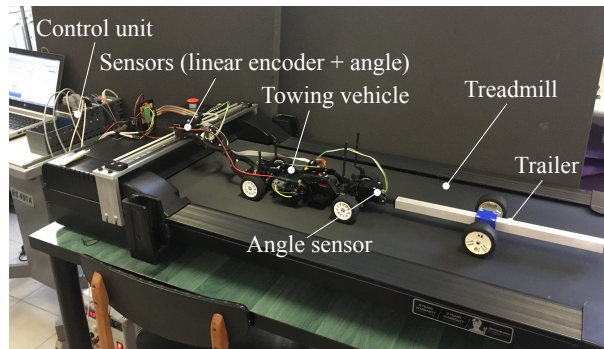


Figure 9. Small-scale experimental rig

### 5.2. Validation

The main purpose of the experiments was to validate the theoretical results of stability charts. The charts are shown in Figure 10(a) for time delay  $\tau = 0.1$  s and in panel (c) for  $\tau = 0.5$  s. The boundaries denoted by black solid lines are calculated as formerly introduced in Section 3.3.3 for zero curvature. Black stars mark the most stable gain

configurations in a theoretical sense. Furthermore, black dashed lines represent the theoretical stability boundary related to a model that neglects the dynamics of the steering mechanism, see Section 3.3.1. As shown, this simplified model significantly overestimates the size of the stable domain.

According to the tests, the green dots represent the configurations for stable motion, and the red crosses for unstable motion. The stable or unstable nature of the motion was decided based on the observed motion of the vehicle that was also captured by the measured time histories. For example, the increasing oscillation amplitudes represent unstable motions in Figure 11.

In Figure 10, there is a qualitative agreement between the theoretical and the experimental results for both (a) moderate ( $\tau = 0.1$  s) and (c) significant ( $\tau = 0.5$  s) values of time delay, however, a smaller stable domain is observable from the results of the tests. On the one hand, it is probably caused by dry friction and clearance in the steering mechanism, namely, there is a threshold in reacting that cannot be reached if the control gains are too small. On the other hand, nonlinearities may have relevant effects in the high-gain region (see [25]).

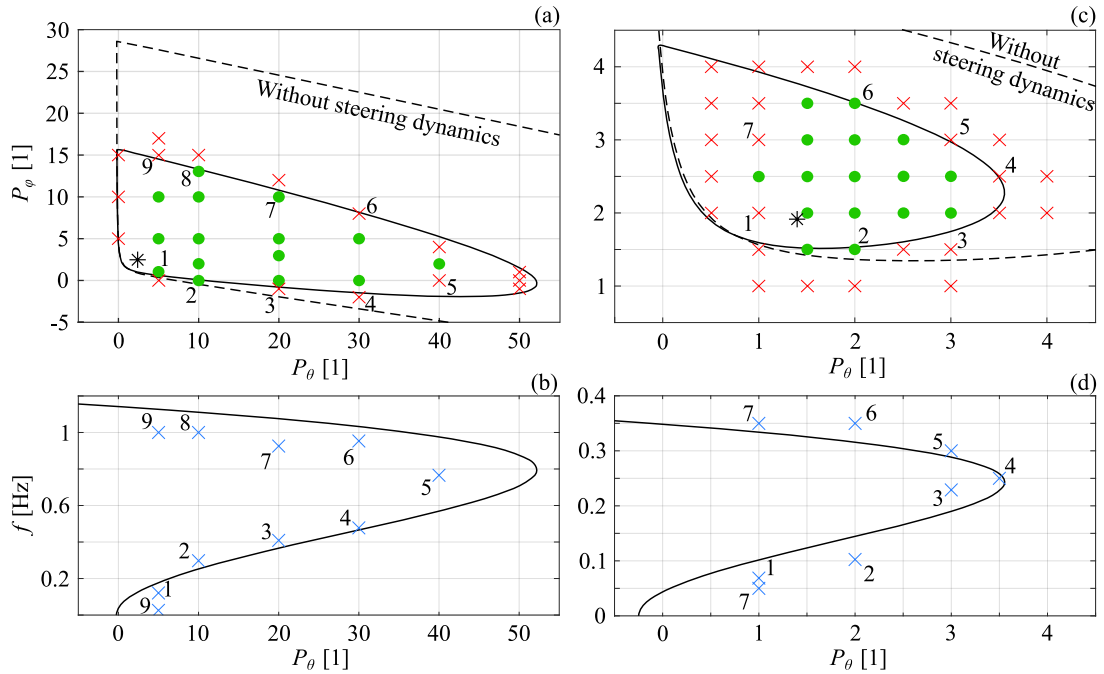


**Figure 10.** Experimental validation of theoretical stability charts in the case of (a) moderate time delay  $\tau = 0.1$  s and (c) significant time delay  $\tau = 0.5$  s. Gain related to the lateral position is  $P_e = -5$  1/m. Black solid and black dashed lines represent the theoretical stability boundary when steering dynamics are included and neglected, respectively. Measurements relate to green dots referring to stable motion and to red crosses referring to unstable motion. Black star denotes the theoretically most stable gain configuration. Panels (b) and (d) show the theoretical vibration frequencies (black solid line) along the stability boundary with experimental validation (blue crosses) for  $\tau = 0.1$  s and for  $\tau = 0.5$  s, respectively.

### 5.3. Frequency analysis

Time series recorded by the sensors allow us to observe the frequency of the oscillation at which the motion becomes unstable along the stability boundaries. For example, Figure 11(a)–(c) and (d)–(f) show the recorded time series and corresponding spectra

of measurement Point 1 and Point 7 of Figure 10(c), respectively. The fast Fourier transforms (FFT) are calculated based on the yaw angle error signals  $\theta$ . The frequency values of the detected peaks of the spectra are compared to theoretical vibration frequencies, which are analytically calculated by the D-subdivision method [23].

The spectral analysis with its validation is shown in Figure 10(b) and (d) for time delay  $\tau = 0.1$  s and for  $\tau = 0.5$  s, respectively. The theoretical vibration frequencies are plotted with a black curve that refers to the imaginary part of the characteristic exponent situated on the imaginary axis at the stability boundary. Blue crosses show the experimentally detected vibration frequencies on the same graph. For identification purposes, measurement points for control gain setups are numbered in both panels. Note that at the top-left corners of the stable domains in Figure 10(a) and (c), the stability boundary intersects itself, and a possible so-called double Hopf bifurcation emerges. The corresponding measured spectrum is plotted in Figure 11(f), where two distinct frequency values appear that are also marked for the measurement Point 7 in Figure 10(d). The same consideration explains the double frequency at measurement Point 9 in Figure 10(b) for the smaller time delay.

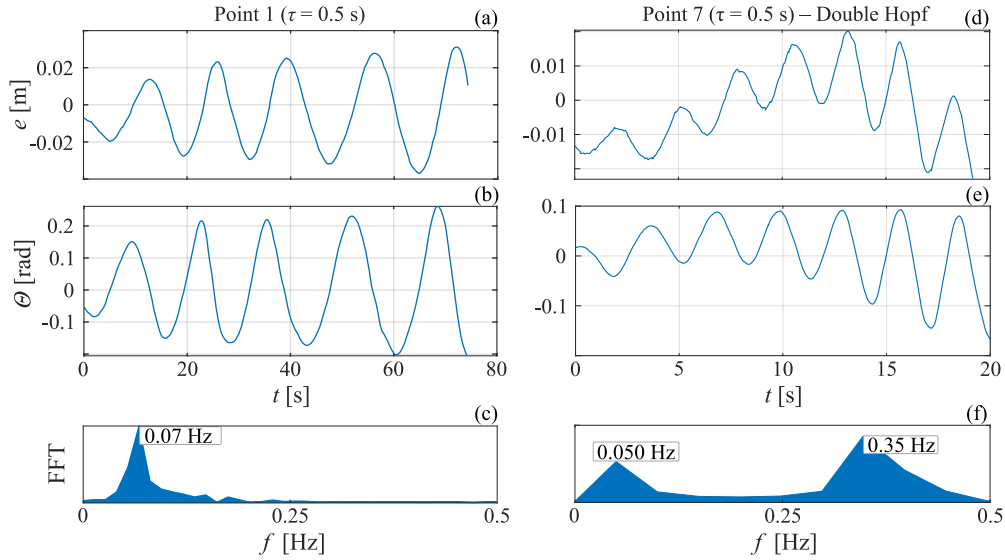


**Figure 11.** Time histories and spectra related to two different scenarios: (a)–(c) Unstable motion at Point 1 of Figure 10(c)–(d) ( $\tau = 0.5$  s,  $P_e = -5$  rad/m,  $P_\theta = 1$  and  $P_\varphi = 2$ ); (d)–(f) Double Hopf bifurcation at Point 7 of Figure 10(c)–(d) ( $\tau = 0.5$  s,  $P_e = -5$  rad/m,  $P_\theta = 1$  and  $P_\varphi = 3$ ).

## 6. Conclusion

The path-following problem of a truck–semitrailer was investigated in the case of reversing using the single-track kinematic model with steering dynamics. A two-level controller was designed and tuned based on linear stability charts of the constant curvature path-following. The effect of time delay and path curvature on stability were highlighted. An adaptive gain tuning method was introduced to control the vehicle system on a path with varying curvature.

The performance of the controller was verified via numerical simulations. The assumption of constant curvature in the model probably causes the lateral deviation of the simulated trajectory from the desired path. The performance would be improved

if the changing rate of the curvature could be considered, which is a complicated task. Improved accuracy also could be reached using a more complicated controller. Methods based on fuzzy logic [26] or Model Predictive Control [27] can optimize path-following in real-time, but guaranteeing the stability of these controllers is not trivial.

However, as the simulation results show, our simple linear controller can be sufficient with less computing power. It is suitable for realizing complicated maneuvers in reverse, even with varying curvature. In such cases, the use of adaptive control gains is recommended, especially when the control system is burdened with significant time delay. Furthermore, stability of the motion can also be ensured in the case of constant curvatures. The relevance of the introduced controller is also strengthened via our experiments on the small-scale test rig. The theoretical vibration frequencies at stability loss were also validated experimentally, even when two vibration frequencies emerged close to the theoretically predicted double Hopf bifurcation point.

## Acknowledgement

The research has been supported by the National Research, Development, and Innovation Office under grant no. 2020-1.2.4-TET-IPARI-2021-00012 and no. NKFI-146201. The project has received funding from the HUN-REN Hungarian Research Network. D.T. is supported by the Janos Bolyai Research Scholarship of the Hungarian Academy of Sciences.

## References

- [1] Ziaukas Z, Wielitzka M, Ortmaier T, et al. Simultaneous estimation of steering and articulation angle in a truck-semitrailer combination solely based on trailer signals. In: 2019 American Control Conference (ACC); 2019. p. 2509–2514.
- [2] Ploeg J, van de Wouw N, Nijmeijer H.  $\mathcal{L}_p$  string stability of cascaded systems: Application to vehicle platooning. *IEEE Transactions on Control Systems Technology*. 2014;22(2):786–793.
- [3] Feng S, Zhang Y, Li SE, et al. String stability for vehicular platoon control: Definitions and analysis methods. *Annual Reviews in Control*. 2019;47:81–97.
- [4] Chiu J, Goswami A. The critical hitch angle for jackknife avoidance during slow backing up of vehicle–trailer systems. *Vehicle System Dynamics*. 2014;52(7):992–1015.
- [5] Hejase M, Jing J, Maroli JM, et al. Constrained backward path tracking control using a plug-in jackknife prevention system for autonomous tractor-trailers. In: 21st International Conference on Intelligent Transportation Systems (ITSC); 2018. p. 2012–2017.
- [6] Ritzen P, Roebroek E, van de Wouw N, et al. Trailer steering control of a tractor–trailer robot. *IEEE Transactions on Control Systems Technology*. 2016;24(4):1240–1252.
- [7] Kural K, Hatzidimitris P, van de Wouw N, et al. Active trailer steering control for high-capacity vehicle combinations. *IEEE Transactions on Intelligent Vehicles*. 2017;2(4):251–265.
- [8] Widoyatriatmo A, Nazaruddin YY, Putranto MRF, et al. Forward and backward motions path following controls of a truck-trailer with references on the head-truck and on the trailer. *ISA Transactions*. 2020;105:349–366.
- [9] Hafner M, Pilutti T. Control for automated trailer backup. In: SAE Technical Paper 2017-01-0040; 04; 2017.
- [10] Li B, Acarman T, Zhang Y, et al. Tractor-trailer vehicle trajectory planning in narrow environments with a progressively constrained optimal control approach. *IEEE Transactions on Intelligent Vehicles*. 2020;5(3):414–425.

- [11] Shin H, Kim MJ, Baek S, et al. Perpendicular parking path generation and optimal path tracking algorithm for auto-parking of trailers. *International Journal of Control, Automation and Systems*. 2022;20(9):3006–3018.
- [12] Cheng J, Zhang Y, Wang Z. Path tracking control for mobile robot with two trailers. In: *Proceedings of the 32nd Chinese Control Conference*; 2013. p. 4337–4341. Available from: <https://ieeexplore.ieee.org/document/6640182>.
- [13] Marcin Michałek M. A highly scalable path-following controller for N-trailers with off-axle hitching. *Control Engineering Practice*. 2014;29:61–73.
- [14] Chung W, Park M, Yoo K, et al. Backward-motion control of a mobile robot with n passive off-hooked trailers. *Journal of Mechanical Science and Technology*. 2011;25(11):2895–2905.
- [15] Bertolazzi E, Frego M. On the G2 Hermite interpolation problem with clothoids. *Journal of Computational and Applied Mathematics*. 2018;341:99–116.
- [16] Pacejka HB. *Tire and vehicle dynamics*, third edition. Butterworth–Heinemann, Oxford; 2012.
- [17] Werling M, Reinisch P, Heidingsfeld M, et al. Reversing the general one-trailer system: Asymptotic curvature stabilization and path tracking. *IEEE Transactions on Intelligent Transportation Systems*. 2014;15(2):627–636.
- [18] Qin WB, Zhang Y, Takacs D, et al. Nonholonomic dynamics and control of road vehicles: moving toward automation. *Nonlinear Dynamics*. 2022 sep;110(3):1959–2004.
- [19] Beregi S, Avedisov SS, He CR, et al. Connectivity-based delay-tolerant control of automated vehicles: Theory and experiments. *IEEE Transactions on Intelligent Vehicles*. 2023; 8(1):275–289.
- [20] Fliess M, Lévine J, Martin P, et al. Flatness and defect of non-linear systems: introductory theory and examples. *International Journal of Control*. 1995;61(6):1327–1361.
- [21] Rouchon P, Fliess M, Levine J, et al. Flatness, motion planning and trailer systems. In: *Proceedings of 32nd IEEE Conference on Decision and Control*; 1993. p. 2700–2705 vol.3.
- [22] Zhou S, Zhang S. Lateral stability control on tractor semi-trailer based on anti-jackknife apparatus. In: *2014 IEEE Conference and Expo Transportation Electrification Asia-Pacific (ITEC Asia-Pacific)*; 2014. p. 1–6.
- [23] Insperger T, Stépán G. *Semi-discretization for time-delay systems—stability and engineering applications*. Springer New York, NY; 2011.
- [24] Berjoza D. Research in kinematics of turn for vehicles and semi-trailers. *Engineering for Rural Development*. 2008 01; Available from: <https://api.semanticscholar.org/CorpusID:59580500>.
- [25] Vörös I, Takács D. Lane-keeping control of automated vehicles with feedback delay: Non-linear analysis and laboratory experiments. *European Journal of Mechanics - A/Solids*. 2022;93:104509.
- [26] Gómez-Bravo F, Cuesta F, Ollero A, et al. Continuous curvature path generation based on  $\beta$ -spline curves for parking manoeuvres. *Robotics and Autonomous Systems*. 2008; 56(4):360–372.
- [27] Cai H, Xu X. Lateral stability control of a tractor-semitrailer at high speed. *Machines*. 2022;10(8).

## Appendix A.

Let us introduce the parameters:

$$v := \frac{V}{l} (l \cos \varphi^* - a \sin \varphi^* \tan \delta_{\text{ff}}) ,$$

$$r := -\frac{Va}{lL \cos^2 \delta_{\text{ff}}} .$$

Using these, the system matrix  $\mathbf{A}$  and the control input vector  $\mathbf{B}$  of the state-space representation in (32) can be represented as shown in (A1) and (A2), respectively.

$$\mathbf{A} = \begin{bmatrix} 0 & v & 0 & 0 & 0 \\ -v\kappa^2 & 0 & V\kappa \left( \sin \varphi^* + \frac{a}{l} \tan \delta_{\text{ff}} \cos \varphi^* \right) - \frac{v}{L} & r (\cos \varphi^* - \kappa L \sin \varphi^*) & 0 \\ 0 & 0 & -\frac{v}{L} & r \left( \cos \varphi^* + \frac{L}{a} \right) & 0 \\ 0 & 0 & 0 & 0 & 1 \\ 0 & 0 & 0 & -p & -d \end{bmatrix}, \quad (\text{A1})$$

$$\mathbf{B} = [0 \ 0 \ 0 \ 0 \ p]^T. \quad (\text{A2})$$